Supplemental Material

A superconducting boron allotrope featuring anticlinal pentapyramids

Zhi Cui[1†], Qiuping Yang[1,2†], Xin Qu[3†], Xiaohua Zhang[1,2], Yong Liu[1], and Guochun Yang[1,2,3,*]

[1]*State Key Laboratory of Metastable Materials Science & Technology and Key Laboratory for Microstructural Material Physics of Hebei Province, School of Science, Yanshan University, Qinhuangdao 066004, China*

[2]*Centre for Advanced Optoelectronic Functional Materials Research and Key Laboratory for UV Light-Emitting Materials and Technology of Northeast Normal University, Changchun 130024, China*

[3]*Key Laboratory of Functional Materials Physics and Chemistry of the Ministry of Education, Key Laboratory of Preparation and Application of Environmental Friendly Materials, College of Physics, Jilin Normal University, Changchun 130103, China*

[*]Corresponding Author Email: yanggc468@nenu.edu.cn

Index **Page**

Computational Details

The structure search approach is based on a global minimization of free energy surfaces merging *ab initio* total-energy calculations as implemented in the CALYPSO code[1, 2]. We have performed extensive structure searches on the Sr-B system with various SrB_x (x =1-8) chemical compositions at 0 K and selected pressures of 1 atm, 25, 50, 100, 150, and 200 GPa. Here, the cell size is up to four formula units for SrB_x (x = 1-4) stoichiometries, and two formula units for the other compositions. In the first step, random symmetric structures are constructed in which atomic coordinates are generated by the crystallographic symmetry operations. Local optimizations using the VASP code[3] are performed with the conjugate gradient method, and are deemed to be converged when the enthalpy changes become smaller than 1×10^{-5} eV per cell. The cut-off energy for the expansion of wavefunctions into plane waves is set to 370 eV and a Monkhorst–Pack k-mesh with a maximum spacing of $2\pi \times 0.06$ Å^{-1} was used in all structure searches. After the first generation of structures is optimized 60% of the lowest lying structures are selected to construct the next generation by PSO (Particle Swarm Optimization). 40% of the structures in the new generation are randomly generated. A structure fingerprinting technique using a bond characterization matrix is applied to the generated structures, so that identical structures are strictly forbidden. This procedure significantly enhances the diversity of the structures, which is crucial for maintaining the efficiency of the global search. In most cases, structure search simulations for each calculation are stopped after generating 1000 ~ 1200 structures (e.g., about 20 ~ 30 generations).

In order to further test the reliability of the adopted pseudopotentials for Sr and B, the validity of the projector augmented wave pseudopotentials from the VASP library are checked by comparing the calculated Birch-Murnaghan equation of state with those obtained using the full-potential linearized augmented plane-wave method (LAPW, as implemented in WIEN2k), which employs local orbitals[4]. The Birch-Murnaghan equation of states derived from PAW and LAPW methods are almost identical. Thus, our adopted pseudopotentials are reliable in the range of 0 – 200 GPa.

The electron-phonon coupling calculations are carried out with the density functional perturbation (linear response) theory as implemented in the QUANTUM ESPRESSO package[5]. We employ ultrasoft pseudopotentials with $4s^2 4p^6 5s^2$ and $2s^2 2p^1$ as valence electrons for Sr, and B atoms, respectively. To reliably calculate the electron-phonon coupling in metallic systems, we need to sample dense *k*-meshes for the electronic Brillouin zone integration and enough *q*-points for evaluating the average contributions from the phonon modes: we use a *k*-grid with a spacing of $2\pi \times 0.03$ Å^{-1}. We have calculated the superconducting T_c of Sr as estimated from the McMillan-Allen-Dynes formula[6-8]:

$$T_c = \frac{\omega_{\log}}{1.2} \exp\left[-\frac{1.04(1+\lambda)}{\lambda - \mu^*(1+0.62\lambda)} \right] \qquad (1)$$

where μ^*, the Coulomb pseudopotential, was assumed to be 0.1. The electron-phonon coupling constant, λ, and the logarithmic average phonon frequency, $\omega_{\log}$, are calculated from the Eliashberg spectral function for the electron-phonon interaction:

$$\alpha^2 F(\omega) = \frac{1}{N(E_F)} \sum_{kq,v} \left| g_{k,k+q,v} \right|^2 \delta(\varepsilon_k) \delta(\varepsilon_{k+q}) \delta(\omega - \omega_{q,v}) \qquad (2)$$

where $\lambda = 2\int d\omega \frac{\alpha^2 F(\omega)}{\omega}$; $\omega_{\log} = \exp\left[\frac{2}{\lambda} \int \frac{d\omega}{\omega} \alpha^2 F(\omega) \ln(\omega) \right]$. Herein, $N(E_F)$ is the electronic density of states at the Fermi level, $\omega_{q,v}$ is the phonon frequency of mode *v* and wave vector *q*, and $|g_{k,k+q,v}|$ is the electron-phonon matrix element between two electronic states with momenta *k* and *k* + *q* at the Fermi leve[9].

Supplemental Figures

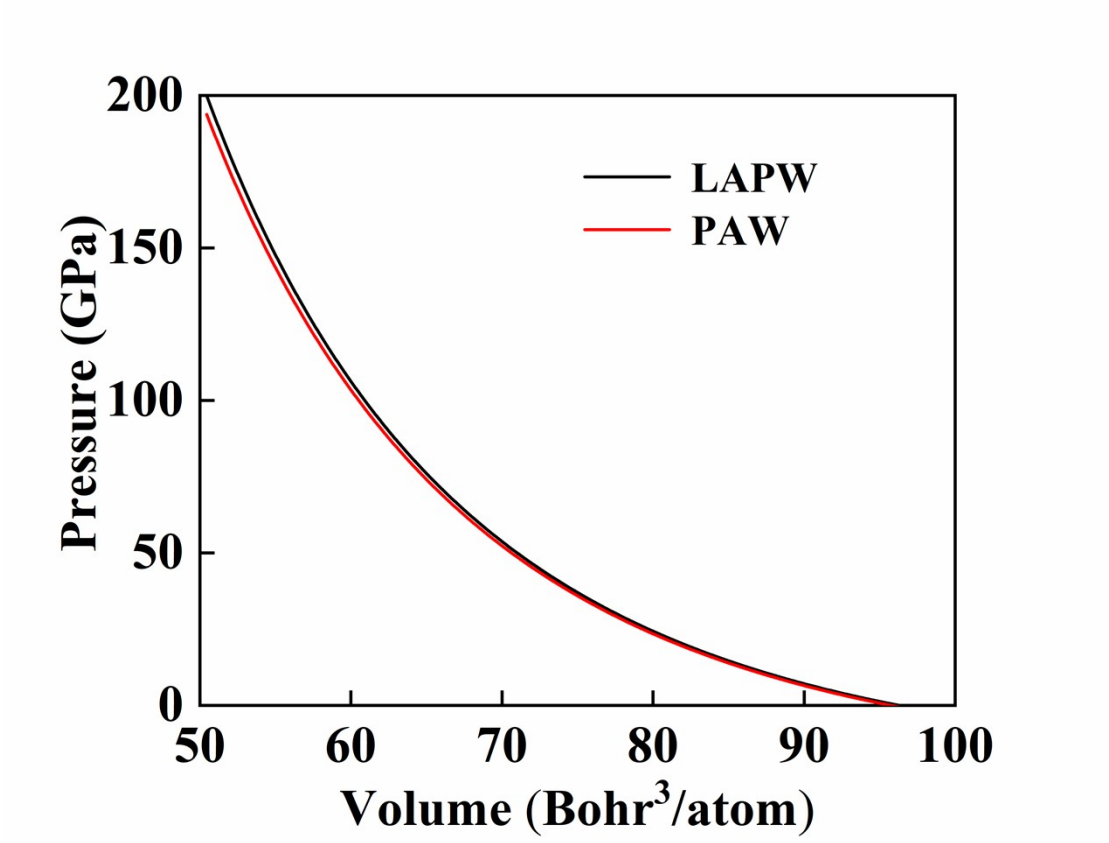

Fig. S0. Comparison of the fitted Birch-Murnaghan equation of states for SrB_2 with *Immm* symmetry by using the results calculated using the PAW pseudopotentials and the full-potential LAPW method.

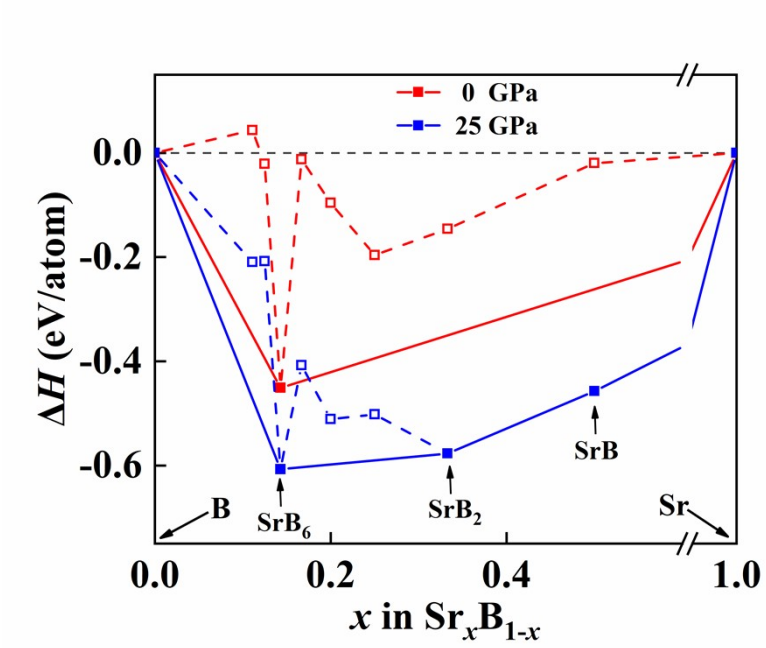

Fig. S1. Phase stabilities of the Sr-B compounds with respect to elemental Sr and B solids at different pressures.

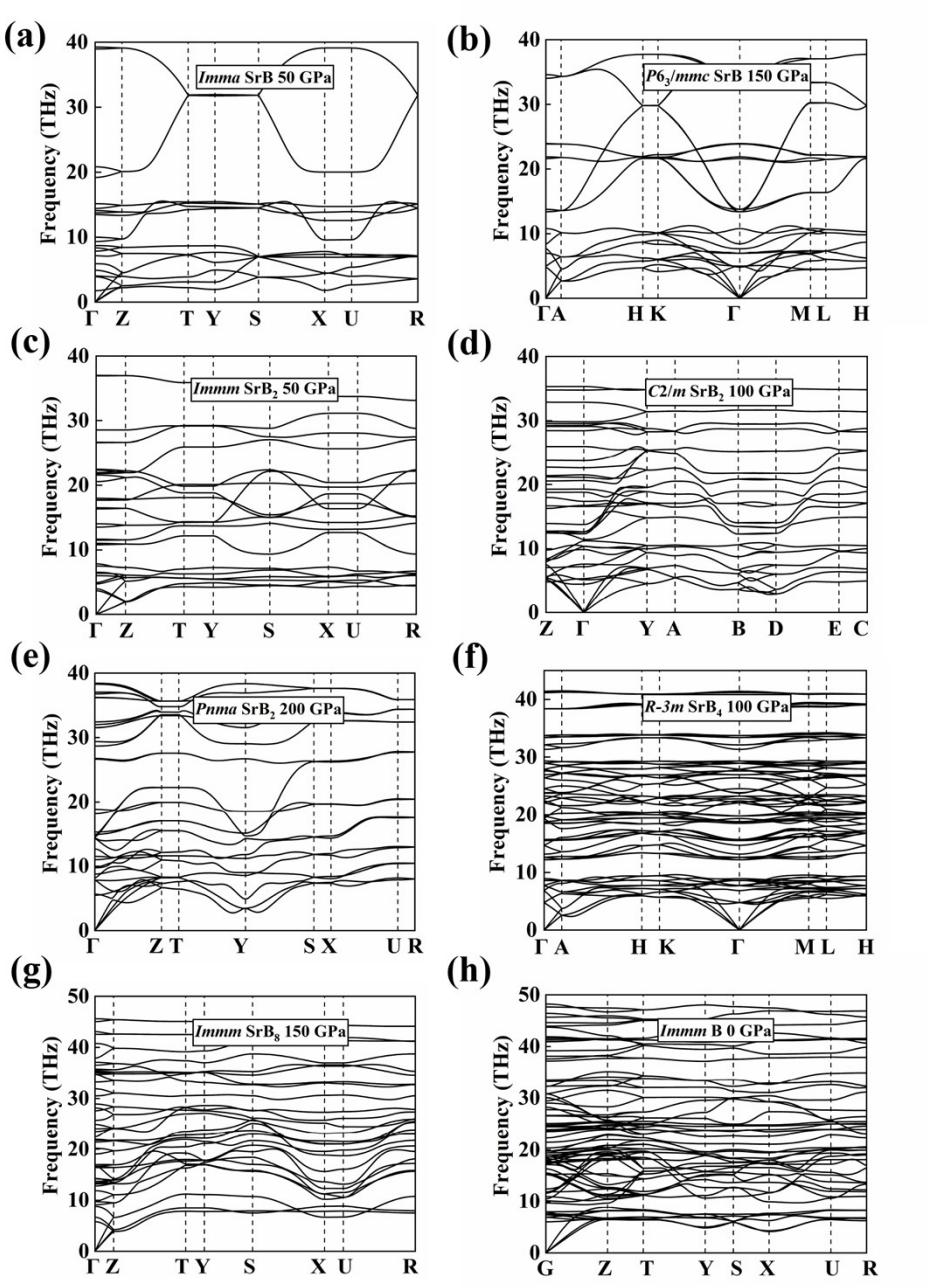

Fig. S2. Phonon dispersion curves of the predicted Sr-B compound, which are all dynamically stable in view of absence of imaginary frequency modes in the first Brillouin zone.

To understand the electronic properties of the Sr-B compound, we calculate the electronic band structures and the projected density of states (PDOS) of the stable phases. In *R*-3*m* SrB_4, there appears to be a large overlap between the Sr-4*d*; Sr-5*p*; B-2*s*; and B-2*p* states below the Fermi level (Fig. S4f), suggesting there occurs charge transfer from Sr to B, in agreement with ELF (Fig. S5f). *R*-3*m* SrB_4 is an indirect semiconductor with a bandgap of 1.18 eV. Interestingly, all stable compounds except SrB_4 are metal, as shown in Figure S3. For the *Imma* SrB, PDOS analysis shows that Sr-4*d* and B-2*p* orbitals have a major contribution to the Fermi level and have significant hybridization between the Sr-4*d*; Sr-5*p*; and B-2*p* orbitals (Fig. S4a), which is similar to the orbital hybridization in *Cmmm* and *I*4/*mmm* SrB_6. The PDOS of other Sr-B structures can reach the same conclusion (Fig. S4). The electron localization function is shown in Fig S5. The Sr-B bond is ionic, and the B–B bond is covalent.

Given the possible superconductivity of metallic compounds, we explore the superconductivity of the metallic phase of the Sr-B system by using the Macmillan-Allen-Deans formulation of μ^* =0.1. Table S1 lists some relevant features and T_c under high pressure. Among them, *Imma* SrB (structure at 50 GPa, Table S2) shows superconducting with T_c=8.1 K, whereas *Immm* SrB_8 (structure at 150 GPa, Table S2) has the lowest (T_c = 0.2 K). We also use the *Imma*-SrB structure to explore the variation of T_c with pressure, as shown in Table S1. For *Imma*-SrB, as the pressure increases, ω_{log}(K) and N (E_f) increase, but the λ value decreases. The corresponding T_c was also reduced from 8.1 K (50 GPa) to 7.4 K (100 GPa).

Table S1. Superconducting properties of the metallic Sr-B phases.

phases	Pressure (GPa)	T_c(K) μ^*=0.1	N(E_f) (states/Ry)	λ	ω_{log} (K)
Imma-SrB	50	8.1	9.52	0.70	230.79
Imma-SrB	100	7.4	7.99	0.62	286.91
*P*6$_3$/*mmc*-SrB	150	3.8	17.95	0.45	463.11
Immm-SrB_2	50	3.8	8.80	0.46	450.78
*C*2/*m*-SrB_2	100	0.5	7.02	0.32	592.88
Pnma-SrB_2	200	0.2	9.68	0.28	653.40
Immm-SrB_8	150	0.2	4.30	0.28	783.37
o-B_{16}	0	14.2	8.29	0.62	577.11

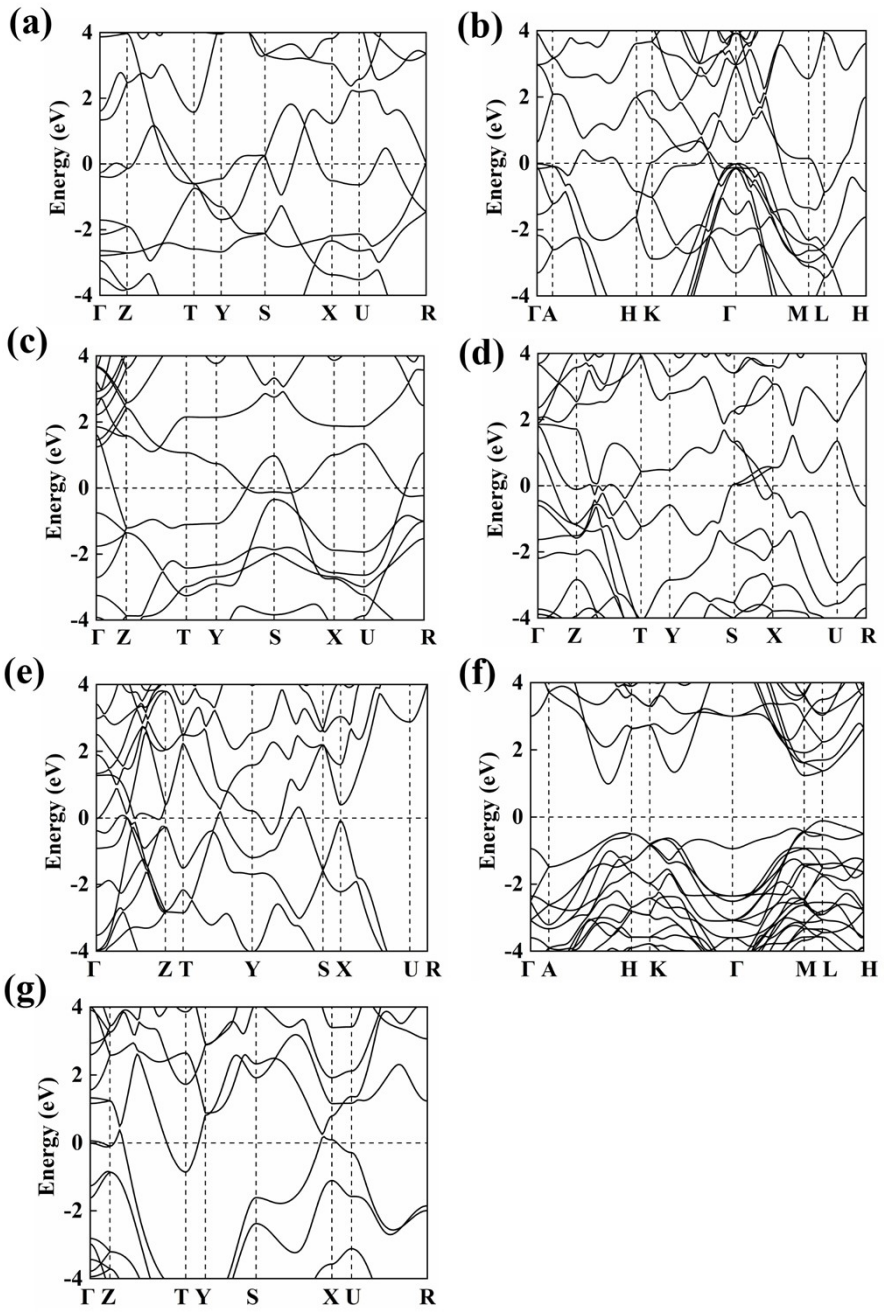

Fig. S3. The electronic band structures of the predicted Sr-B compounds. (a) *Imma* SrB at 50 GPa. (b) $P6_3/mmc$ SrB at 150 GPa. (c) *Immm* SrB_2 at 50 GPa. (d) $C2/m$ SrB_2 at 100 GPa. (e) *Pnma* SrB_2 at 200 GPa. (f) $R\text{-}3m$ SrB_4 at 100 GPa. (g) *Immm* SrB_8 at 150 GPa.

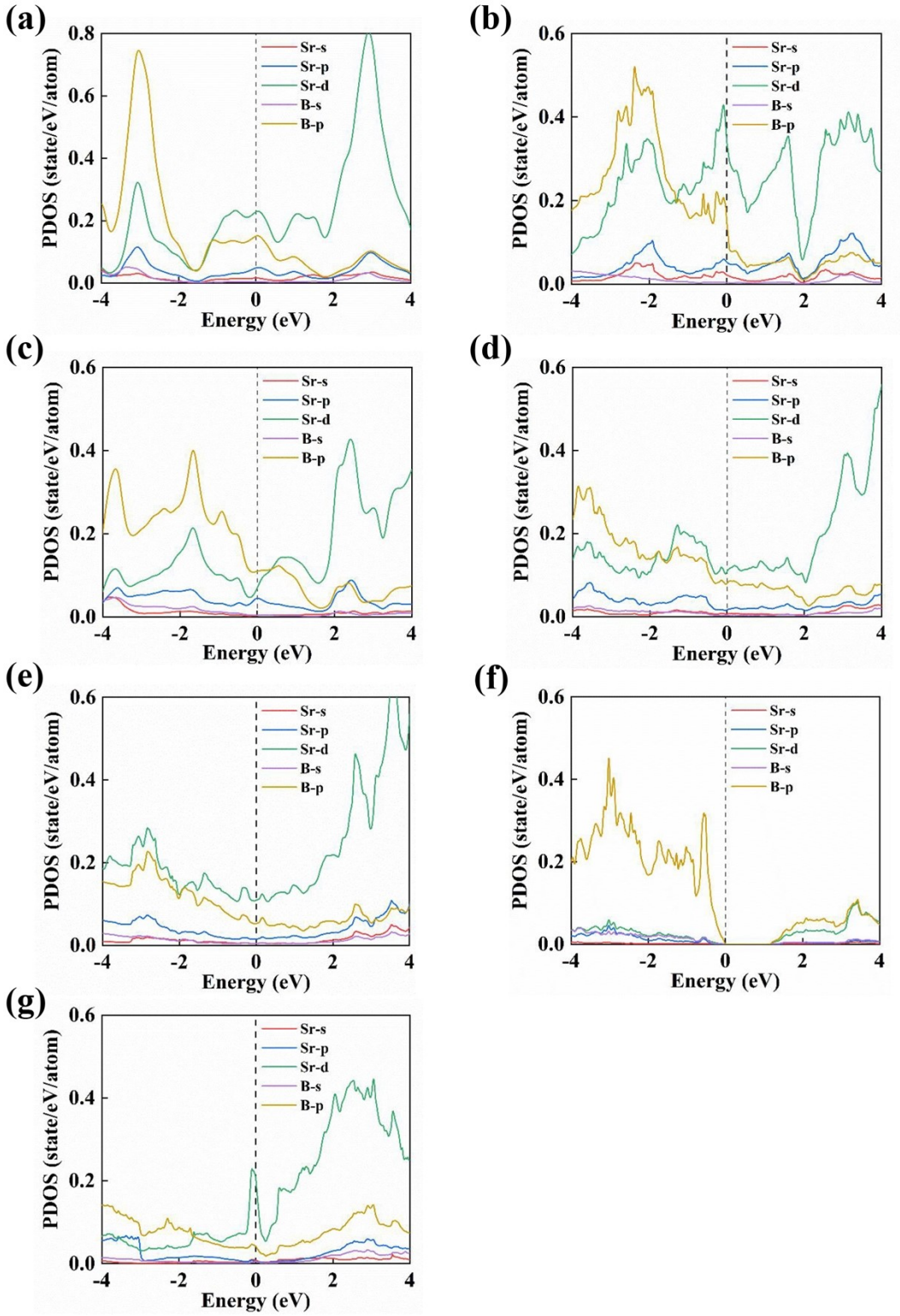

Fig. S4. The projected density of states (PDOS) of the predicted Sr-B compounds. (a) *Imma* SrB at 50 GPa. (b) *P*6$_3$/*mmc* SrB at 150 GPa. (c) *Immm* SrB_2 at 50 GPa. (d) *C*2/*m* SrB_2 at 100 GPa. (e) *Pnma* SrB_2 at 200 GPa. (f) *R*-3*m* SrB_4 at 100 GPa. (g) *Immm* SrB_8 at 150 GPa.

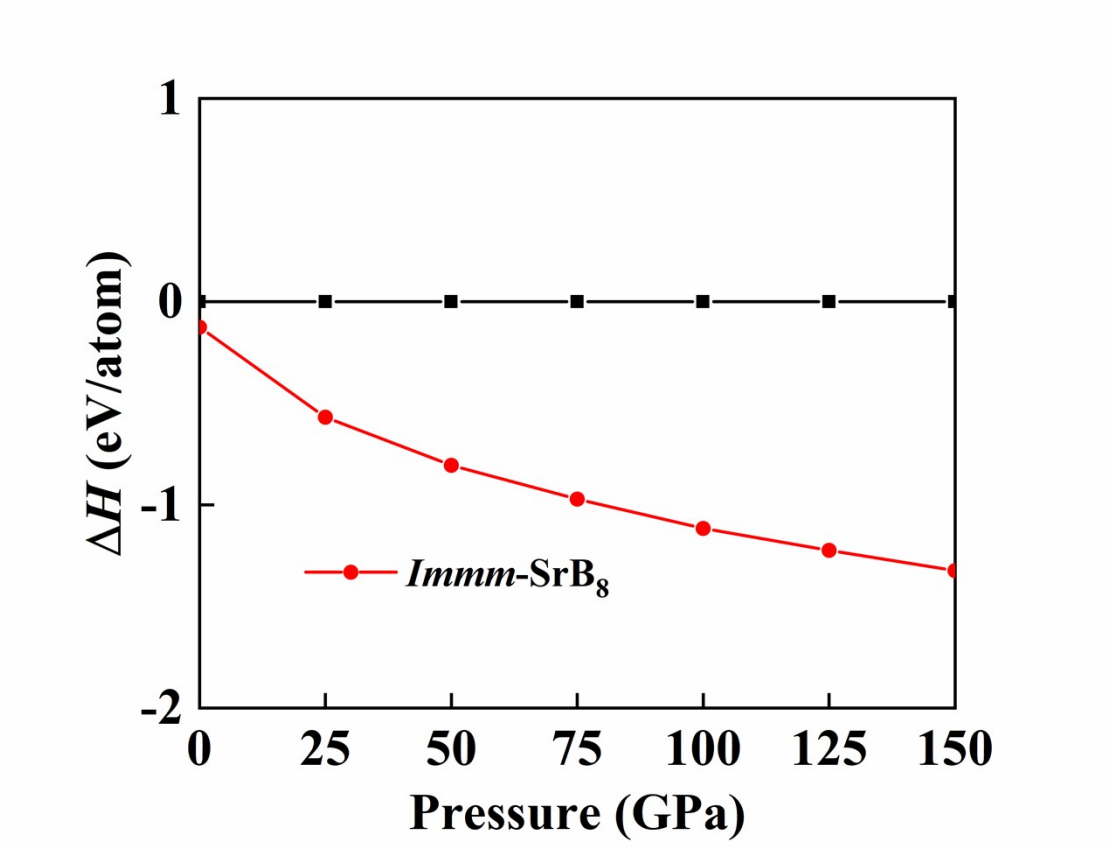

Fig. S5. The formation enthalpy per atom of *Immm*-SrB_8 compounds with respect to Sr and *o*-B_{16} as functions of pressure.

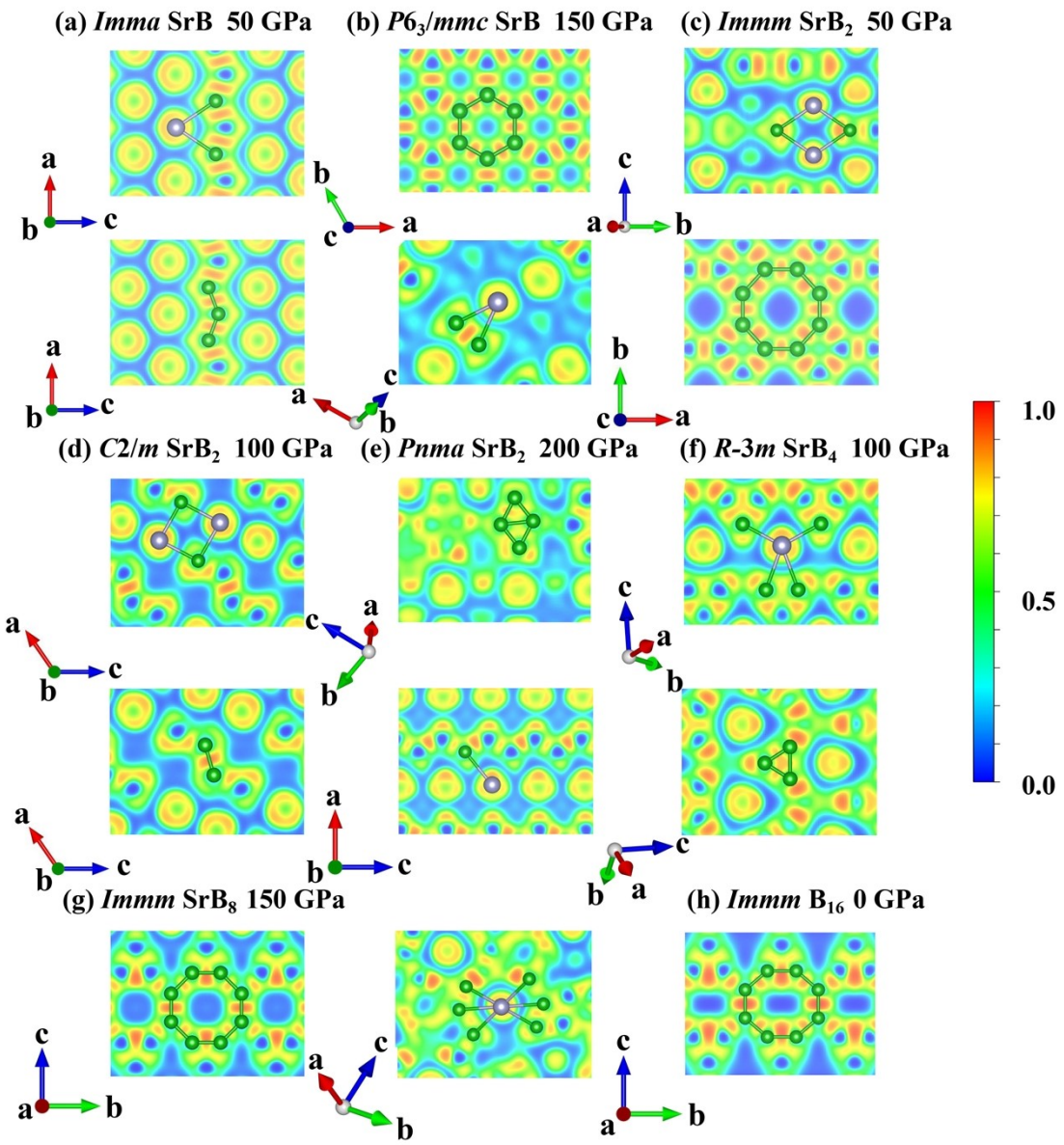

Fig. S6. Electron localization function (ELF) of the predicted stable Sr-B compounds. The ELF analysis can be used to distinguish different types of chemical bonds. Generally, the covalent bonds, lone electron pairs, and core electrons are characterized by large values (> 0.6).

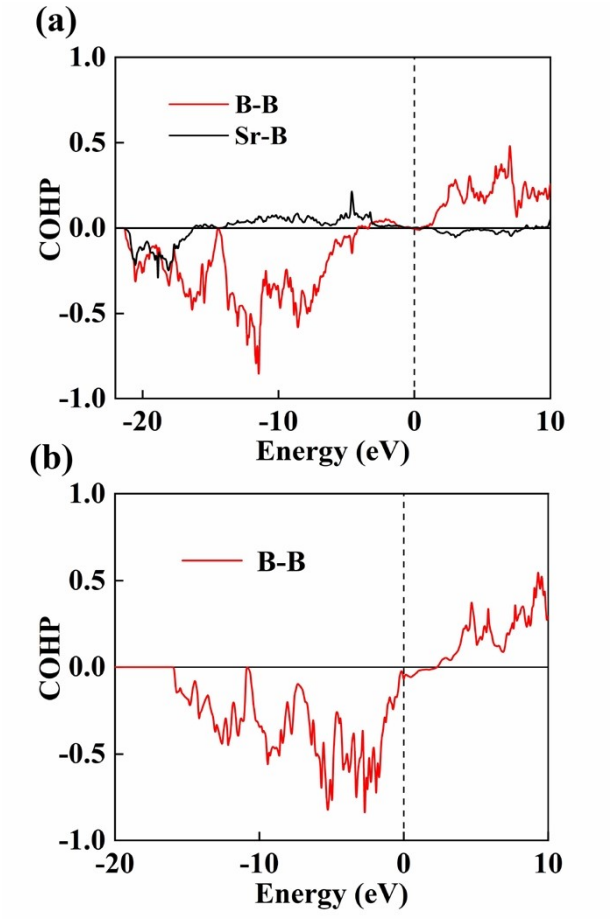

Fig. S7. (a) COHP for *Immm* SrB_8 at 150 GPa. (b) COHP for *Immm* B_{16} at 0 GPa.

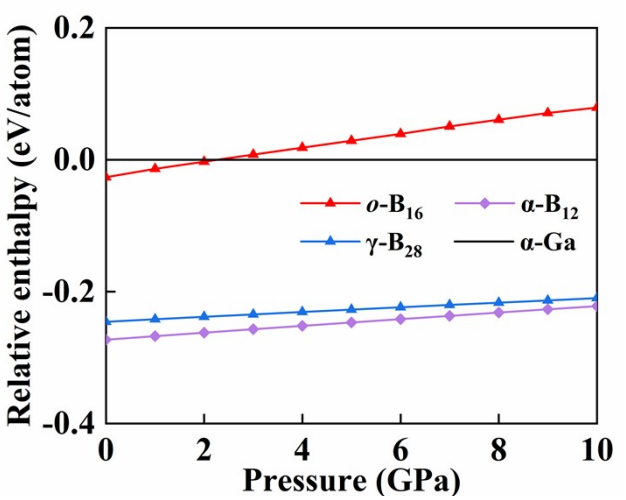

Fig. S8. The relative enthalpy per atom as a function of pressure within PBE calculations at T = 0 K for the considered boron allotropes.

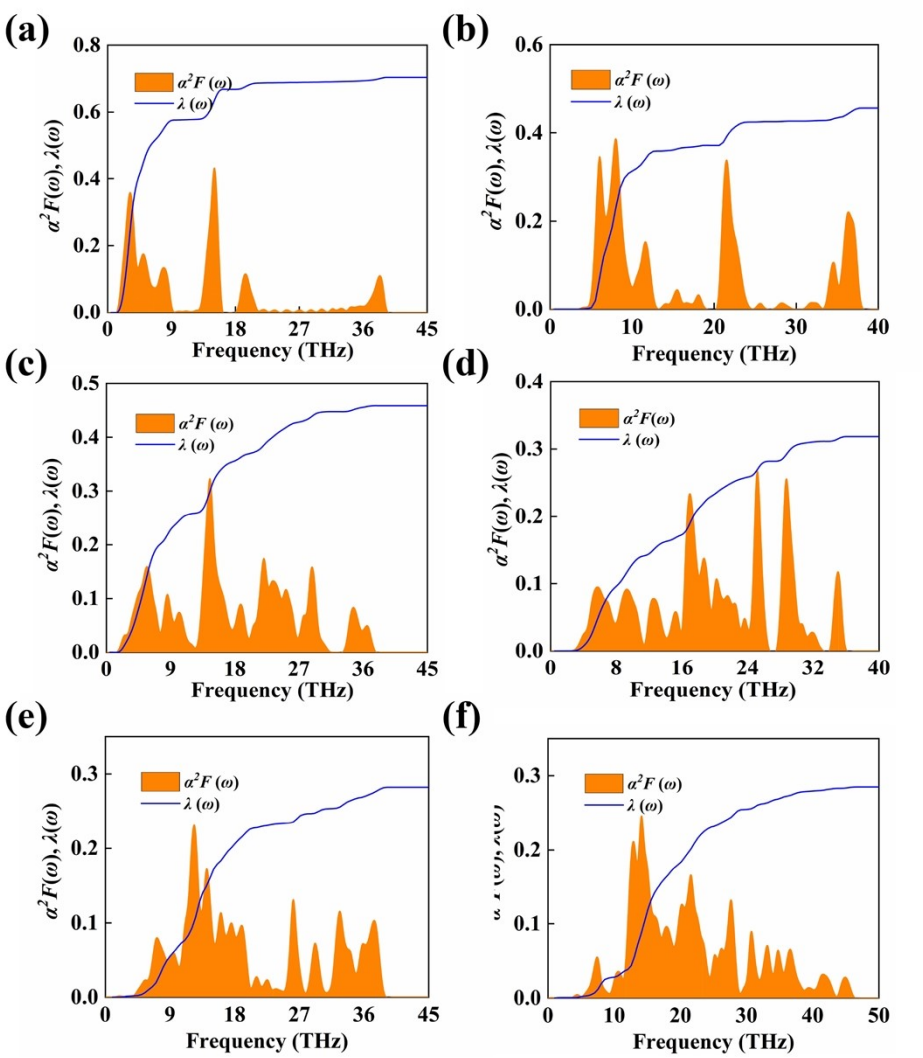

Fig. S9. Eliashberg spectral function $\alpha^2F(\omega)$ (orange area) and frequency-dependent electron-phonon coupling parameters $\lambda(\omega)$ (blue line) of Sr-B compounds. (a) *Imma* SrB at 50 GPa. (b) $P6_3/mmc$ SrB at 150 GPa. (c) *Immm* SrB_2 at 50 GPa. (d) $C2/m$ SrB_2 at 100 GPa. (e) *Pnma* SrB_2 at 200 GPa (f) *Immm* SrB_8 at 150 GPa.

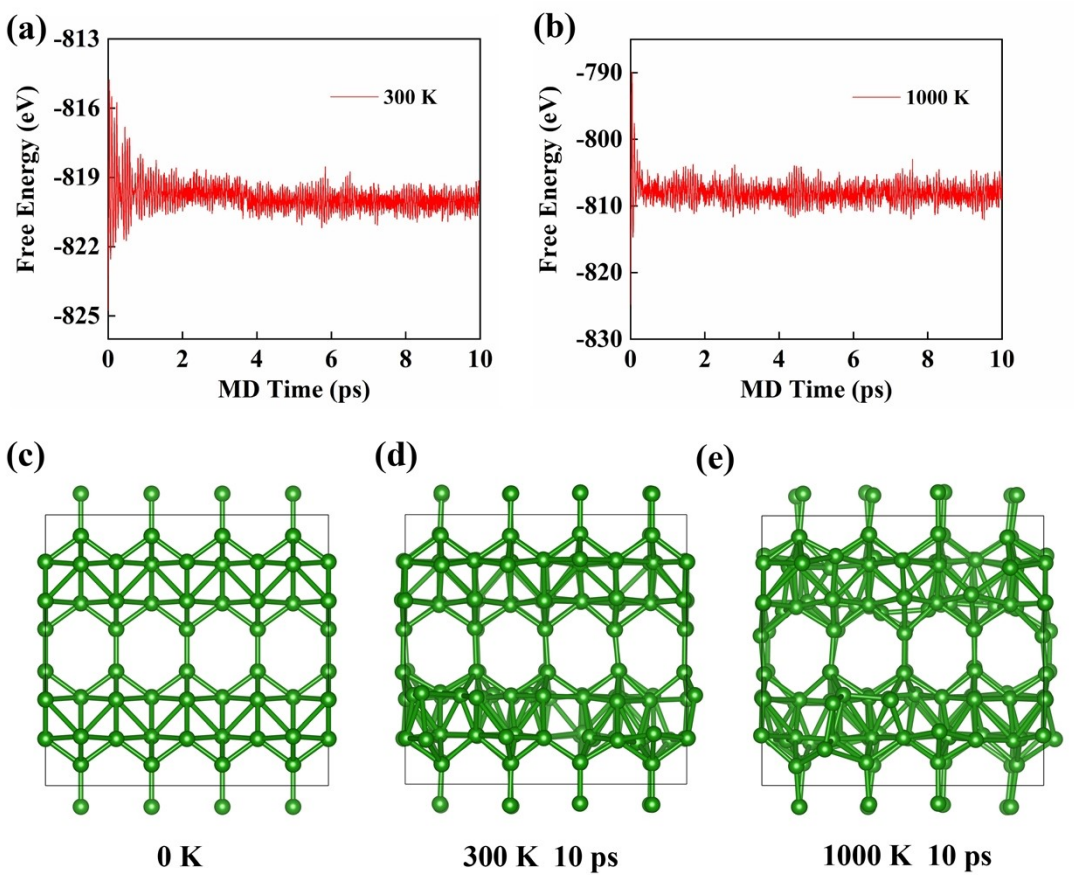

Fig. S10. Free energy as a function of time at the temperatures of 300 and 1000 K for *o*-B_{16} (a, b). Initiating structure (c). Snapshots after equilibration of *o*-B_{16} at 10 ps (d, e).

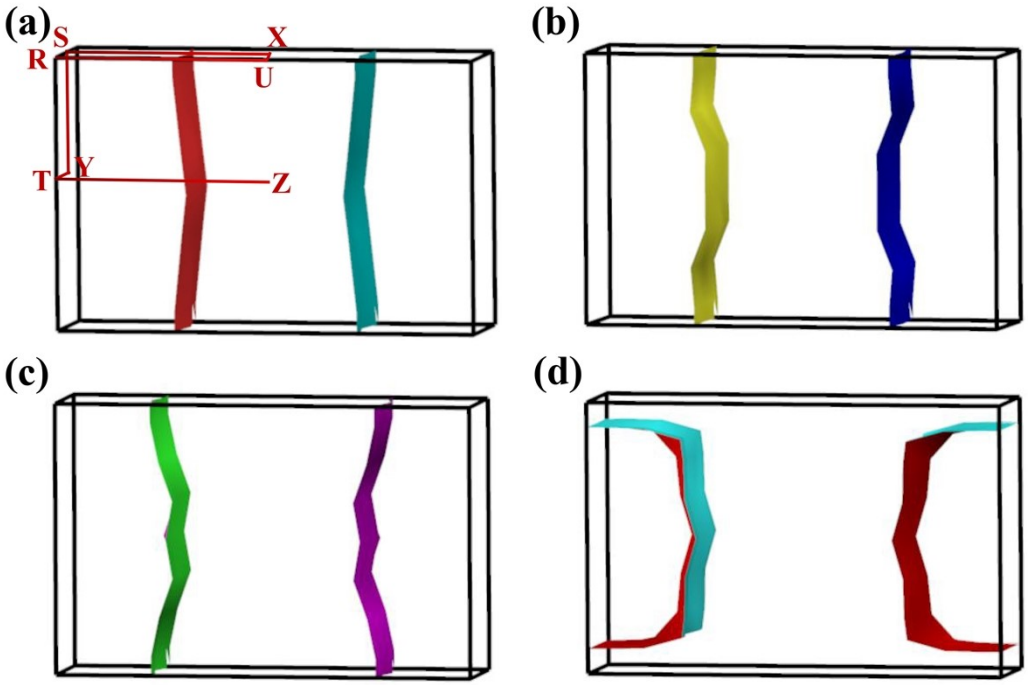

Fig. S11. The *o*-B_{16} fermi surface associated with each band crossing the Fermi level.

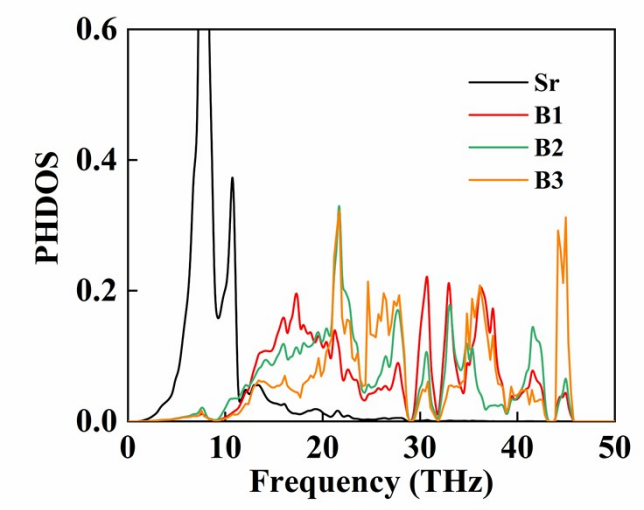

Fig. S12. Phonon density of states (PHDOS) of *Immm* SrB_8.

Table S2. Structural information for the predicted stable Sr-B phases.

Phases	Pressure (GPa)	Lattice Parameters (Å, °)	Atoms	Wyckoff Positions (fractional)		
				x	*y*	*z*
***Imma* SrB**	50	*a* = 2.9761	Sr(4e)	0.00000	0.75000	0.08993
		b = 4.5341	B(4e)	0.50000	1.25000	0.21283
		c = 7.3510				
		α = 90.0000				
		β = 90.0000				
		γ = 90.0000				
***P6$_3$/mmc* SrB**	150	*a* = 2.7595	Sr (4f)	0.66667	0.33333	0.90895
		b = 2.7595	B(2b)	0.00000	0.00000	0.25000
		c = 11.0988	B(2d)	0.33333	0.66667	0.75000
		α = 90.0000				
		β = 90.0000				
		γ = 120.0000				
***Immm* SrB$_2$**	50	*a* = 7.8485	Sr (4e)	-0.19037	0.00000	0.00000
		b = 3.9441	B(4j)	0.00000	-0.50000	0.19648
		c = 4.0766	B(4h)	0.00000	-0.21125	0.50000
		α = 90.0000				
		β = 90.0000				
		γ = 90.0000				
***C*2/*m* SrB$_2$**	100	*a* = 7.7259	Sr(4i)	0.92040	0.50000	0.13560
		b = 2.8307	B(4i)	0.87401	0.00000	0.44329
		c = 5.7547	B(4i)	0.23955	0.00000	0.38560
		α = 90.0000				
		β = 124.8714				
		γ = 90.0000				
***Pnma* SrB$_2$**	200	*a* = 10.9493	Sr(4c)	-0.31999	0.75000	0.77495
		b = 2.7396	B(4c)	0.07317	0.25000	0.19668
		c = 2.8039	B(4c)	0.00163	0.25000	0.69452
		α = 90.0000				
		β = 90.0000				
		γ = 90.0000				
***R-3m* SrB$_4$**	100	*a* = 4.2085	Sr(6c)	0.00000	0.00000	0.79171
		b = 4.2085	B(6c)	0.00000	0.00000	0.56189
		c = 14.2745	B(18h)	-0.39296	-0.19648	0.62204
		α = 90.0000				
		β = 90.0000				
		γ = 120.0000				
***Immm* SrB$_8$**	150	*a* = 2.6147	Sr(2d)	0.00000	0.50000	0.00000
		b = 3.90370	B(4i)	0.00000	0.00000	0.16735
		c = 10.0127	B(8l)	0.00000	0.20288	0.30739

		α = 90.0000	B(4j)	0.50000	0.00000	0.92209
		β = 90.0000				
		γ = 90.0000				
***o*-B_{16}**	0	a = 2.8026	B(4i)	0.00000	0.00000	0.17331
		b = 4.3365	B(8l)	0.00000	0.19774	0.31764
		c = 10.71920	B(4j)	0.50000	0.00000	0.92191
		α = 90.000				
		β = 90.000				
		γ = 90.000				

Table S3. Elastic stiffness constants C_{ij}.

	C_{11}	C_{22}	C_{33}	C_{44}	C_{55}	C_{66}	C_{12}	C_{13}	C_{23}
o-B_{16}	460.07	536.28	483.15	124.22	109.85	61.35	16.80	25.82	97.58

The criteria for mechanical stability are given by:

$C_{11}>0$, $C_{22}>0$, $C_{33}>0$, $C_{44}>0$, $C_{55}>0$, $C_{66}>0$,

$[C_{11}+C_{22}+C_{33}+2(C_{12}+C_{13}+C_{23})]>0$,

$(C_{11}+C_{22}-2C_{12})>0$,

$(C_{11}+C_{33}-2C_{13})>0$,

$(C_{22}+C_{33}-2C_{23})>0$.

Table S4. Bader atomic charge of the predicted stable Sr-B phases.

Phases	Pressure (GPa)	Atoms	Charge (e)
***Immm* SrB_8**	150	Sr1	1.03
		B1	-0.22
		B2	-0.08
		B3	-0.09

Table S5. Total energy of *o*-B_{16}, *α*-B_{12}, *γ*-B_{28}, and *α*-Ga-type boron.

Phases	Pressure (GPa)	Energy (eV/atom)
***γ*-B_{28}**	0 GPa	-6.6526
***α*-B_{12}**	0 GPa	-6.6798
***α*-Ga-type**	0 GPa	-6.4070
***o*-B_{16}**	0 GPa	-6.4332

References

1. Y. Wang, J. Lv, L. Zhu and Y. Ma, *Phys. Rev. B*, 2010, **82**, 094116.
2. Y. Wang, J. Lv, L. Zhu and Y. Ma, *Comput. Phys. Commun.*, 2012, **183**, 2063-2070.
3. G. Kresse and J. Furthmüller, *Phys. Rev. B*, 1996, **54**, 11169-11186.
4. P. Blaha, K. Schwarz, P. Sorantin and S. B. Trickey, *Comput. Phys. Commun.*, 1990, **59**, 399-415.
5. P. Giannozzi, S. Baroni, N. Bonini, M. Calandra, R. Car, C. Cavazzoni, D. Ceresoli, G. L. Chiarotti, M. Cococcioni, I. Dabo, A. Dal Corso, S. de Gironcoli, S. Fabris, G. Fratesi, R. Gebauer, U. Gerstmann, C. Gougoussis, A. Kokalj, M. Lazzeri, L. Martin-Samos, N. Marzari, F. Mauri, R. Mazzarello, S. Paolini, A. Pasquarello, L. Paulatto, C. Sbraccia, S. Scandolo, G. Sclauzero, A. P. Seitsonen, A. Smogunov, P. Umari and R. M. Wentzcovitch, *J. Phys: Condens. Mat.*, 2009, **21**, 395502.
6. L. N. Oliveira, E. K. U. Gross and W. Kohn, *Phys. Rev. Lett.*, 1988, **60**, 2430-2433.
7. M. Lüders, M. A. L. Marques, N. N. Lathiotakis, A. Floris, G. Profeta, L. Fast, A. Continenza, S. Massidda and E. K. U. Gross, *Phys. Rev. B*, 2005, **72**, 024545.
8. P. B. Allen and R. C. Dynes, *Phys. Rev. B*, 1975, **12**, 905-922.
9. J. P. Carbotte, *Rev.Mod. Phys.*, 1990, **62**, 1027-1157.